PERGAMON

Journal of Structural Geology 21 (1999) 305–312

JOURNAL OF STRUCTURAL GEOLOGY

# Size distribution of clasts in experimentally produced pseudotachylytes

Akito Tsutsumi *

*Earthquake Research Institute, University of Tokyo, 1-1-1 Yayoi, Bunkyo-ku, Tokyo 113, Japan*

Received 28 July 1998; accepted 3 November 1998

**Abstract**

High-velocity frictional experiments on monzodiorite, at sliding rates of 1.3 m/s and at normal stresses of 2 MPa, produced dark 100 μm thick pseudotachylyte layers on the sliding surfaces. The experimentally produced pseudotachylyte contains clasts of various sizes in an ultrafine matrix, similar to the texture observed for natural pseudotachylytes. The size distribution of clasts in the experimental pseudotachylyte obeys a power law of the form: $N = N'(1 + r/r')^{-D}$, where $N$ is the cumulative number of clasts with a size greater than $r$, $r'$ and $D$ are material constants, and $N'$ is a constant that depends on the total number of measurements. The total area of ultrafine-grained clasts in a thin section, estimated from the size distribution is less than 0.5%, whereas the actual area of ultrafine matrix is measured as 60–70% of the total product. This suggests that the matrix cannot be regarded as a product of only comminution processes, consistent with natural pseudotachylytes, and that the ratio of actual area of the ultrafine-grained matrix to the hole product represents almost the ratio of the melt (glass). This estimate is consistent with the ratio of glass determined from an X-ray diffraction analysis. 

## 1. Introduction

The origin of natural pseudotachylytes has been controversial since Wenk (1978) cast doubt on the melt origin of the matrix of pseudotachylytes. This is due to the ultrafine-grained and often devitrified nature of the matrix. Despite numerous studies on the mineralogy and chemistry of pseudotachylytes, few workers have attempted to study the origin of pseudotachylytes from the geometrical viewpoint of clasts contained in the matrix. Shimamoto and Nagahama (1991, 1992), however, presented an argument against the crush origin of pseudotachylytes based on a clast-size distribution analysis. They proposed a method for evaluating the proportion of ultrafine-grained clasts in the fine matrix of a natural pseudotachylyte, using size distribution analysis data of the clasts. Their two-dimensional analysis shows that the area of ultrafine-grained clasts predicted from power-law type clast-size distribution data is smaller by nearly one order of magnitude than the actual measured area of the ultrafine matrix, and they argued that the major part of the matrix of their pseudotachylyte cannot be regarded as crush products.

This method, in turn, is also useful for estimating the ratio of melt products to the whole pseudotachylyte; if the total amount of clasts including the ultrafine component could be calculated, the amount of melt products could be determined simply by subtracting the amount of clasts from the total volume. For most natural pseudotachylytes, however, it is difficult to cross-check this estimation by conventional quantitative analysis of the glass because the glass is altered or devitrified. Experimentally produced pseudotachylytes therefore have an advantage over natural pseudotachylytes in doing quantitative analysis of the pseudotachylyte melt.

In this study, high-velocity frictional experiments were performed to produce synthetic pseudotachylytes and size–distribution analyses of clasts contained in the pseudotachylytes were made. Ratio of produced melt to the whole pseudotachylyte was predicted from the size–distribution data and the predicted ratio of the melt was compared with the actual ratio of the melt determined from an X-ray diffraction analysis.

* Current address: Mechanical Engineering Laboratory, Namiki 1-2, Tsukuba, Ibaraki 305, Japan. E-mail: akitsumi@mel.go.jp

0191-8141/99/$ - see front matter 
PII: S0191-8141(98)00113-8

Table 1
Summary of results of the size distribution analysis

| Experiment number | Normal stress (MPa) | Slip rate (m/s) | Total displacement (m) | Constants of Eq. (2) for the best fit lines in Fig. 2 | | | | | Size range of clasts area calculation | | Area of ultrafine-grained products (%) | |
|---|---|---|---|---|---|---|---|---|---|---|---|---|
| | | | | Measured clasts | $N'$ | $r'$ | $D$ | Correlation coefficient, $R$ | Fine-grained range, ($r_1$,$r_2$) (μm) | Coarse-grained range, ($r_1$,$r_2$) (μm) | Predicted | Measured |
| HFR040 | 2.0 | 1.3 | no data | all | 2592.2 | 3.2 | 3.2 | 0.996 | 0.005, 0.5 | 0.5, 35 | 0.4 | 62.7 |
| HFR069 | 0.8 | 1.3 | 170 | all | 1383.6 | 5.3 | 3.8 | 0.996 | 0.005, 0.5 | 0.5, 32 | 0.23 | 66.5 |
| HFR070 | 0.8 | 1.3 | 379 | all | 3441.0 | 15.1 | 4.5 | 0.998 | 0.005, 0.5 | 0.5, 100 | 0.02 | 72.9 |
| | | | | feldspar | 2151.0 | 25.6 | 6.0 | 0.996 | | | | |
| | | | | magnetite | 1027.0 | 3.3 | 2.4 | 0.997 | | | | |

The aim of this study is to test the size–frequency relationship of clasts in experimentally produced pseudotachylytes, to find the area of melt present in the pseudotachylytes and thereby to discover whether these rocks have a melt origin.

## 2. Experimental details

### 2.1. Starting materials

All experiments were performed on a pair of cylindrical specimens of monzodiorite, 40 mm long with a diameter of 25 mm. The monzodiorite sample used is equigranular with an average 0.3 mm grain size and has no recognizable planar structures such as compositional banding or metamorphic foliation. Monzodiorite consists of k-feldspar, plagioclase, pyroxene, biotite and magnetite.

To analyze the mechanical properties of a simulated fault during torsion experiments, hollow cylindrical specimens should be used to minimize the variation of slip rate and friction across the fault plane (Tsutsumi and Shimamoto, 1997). Solid cylinders were used, however, to collect as much volume of experimental pseudotachylytes as possible for the clast-size distribution analysis. Both side faces of both cylinders were carefully polished using a grinding-wheel so that the faces were at a right angle to the length of the specimen.

### 2.2. Experimental procedures

The frictional experiments were performed using a high-speed rotary-shear frictional testing machine designed by T. Shimamoto (Shimamoto and Tsutsumi, 1994). An air-driven actuator applies an axial force of up to 10 kN to a pair of cylindrical specimens through a ball-spline axis. One specimen is kept stationary and the other specimen is rotated with a servo-motor possessing a transmission power rating of 7.5 kW. The motor develops a maximum revolution rate of 1500 r.p.m. and a maximum torque of 47.8 N m. Rotation is transmitted from the motor to the specimen through an electromagnetic clutch so that rotation of the specimen can be disconnected at any time during the experiment. The machine can produce a normal stress of about 20 MPa and slip rates of 1.3 m/s for solid-cylindrical specimens with outer diameters of 25 mm (cf. Shimamoto and Tsutsumi, 1994).

The normal stresses which can be applied to the specimen are limited primarily to the uniaxial strength of the rock sample. For the case of high-speed frictional sliding experiments, however, the strength of the sample decreases drastically by an effect of thermal fracturing due to rapid frictional heating, especially for

quartzose rocks like granite (Ohtomo and Shimamoto, 1994). Thus the normal stresses applied in this study were low compared to the $\sigma_d > 300$ MPa stress condition estimated for the natural pseudotachylyte generation (Sibson, 1975). To compensate for the low normal stress condition, the total displacement (slip) was about two orders of magnitude larger than the natural seismogenic fault slip, which yields equivalent frictional work to that of natural seismogenic fault slip (Table 1).

All specimens were forced to slide at slip rates of 1.3 m/s and at normal stresses to 2.0 MPa. As the rotation of the motor was transmitted to the specimen by engaging the magnetic clutch, the color of the fault surface gradually changed during slip to light reddish yellow, and in a few seconds frictional melting initiated. The axial load was left unchanged at the end of an experiment until the sliding surface cooled down.

## 3. Microstructure of the experimentally produced pseudotachylyte

After the experiments on monzodiorite the two matching specimens were welded by a black, glass lustrous ~100 μm thick layer (Fig. 1a and b). Thin sections cut normal to the sliding surface were made for observations of textures under an optical microscope and SEM-EDS. The boundary between the host rock and the fault zone (the thin black layer) is quite irregular on a microscopic scale (Fig. 1b). The morphology of mineral grains contained in the host rock immedi-

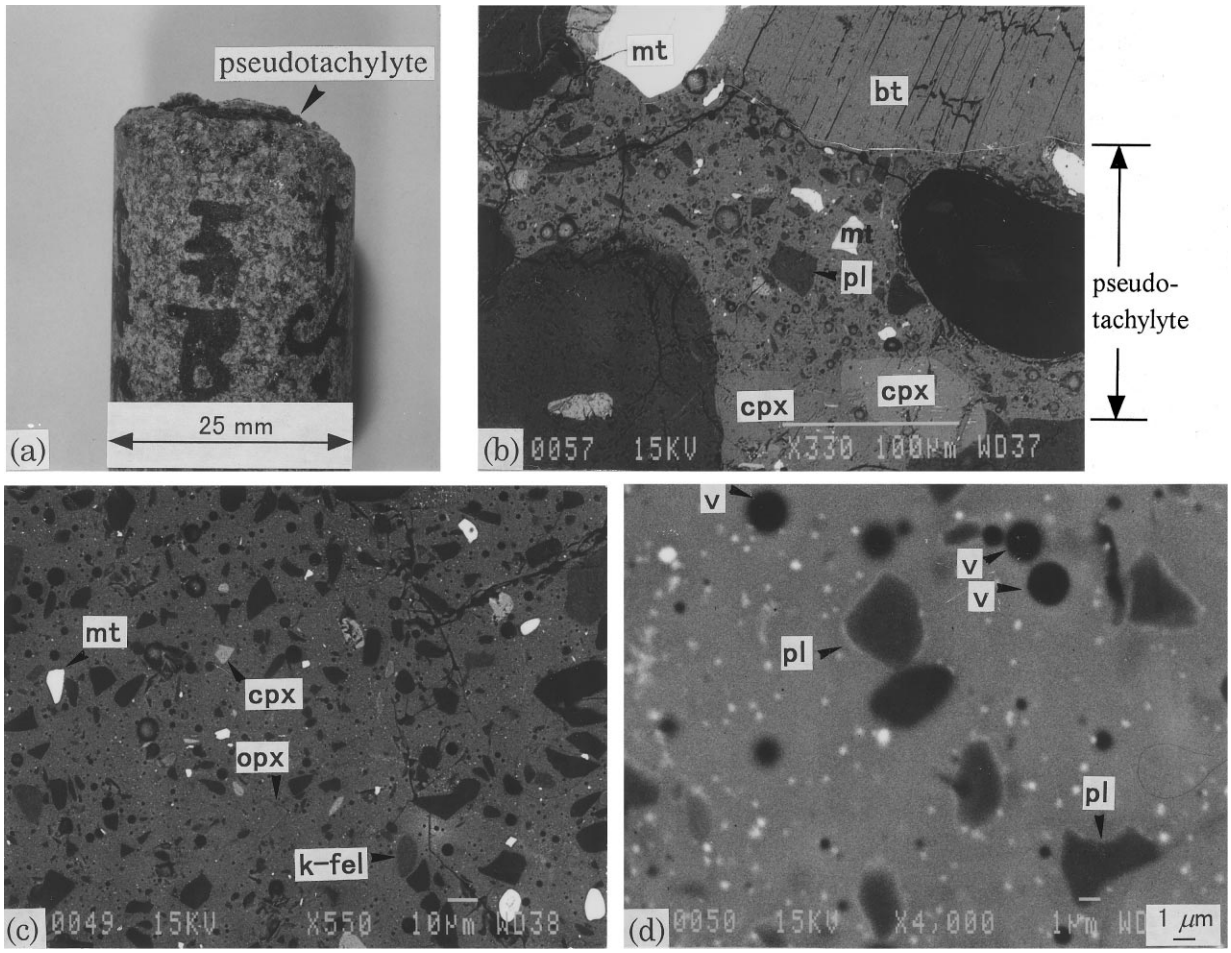


Fig. 1. (a) Deformed specimen of monzodiorite under a normal stress of 0.8 MPa, a slip rate of 1.3 m/s. Note that a fragment of the facing country rock is left on the very top. (b)–(d) Back scattered electron (BSE) images of the experimentally produced pseudotachylyte. Clasts of various sizes are scattered in a fine matrix. (b) BSE image of a thin section cut normal to the sliding surface, showing horizontal boundaries between the host monzodiorite and the pseudotachylyte. A rounded plagioclase occurs in the host rock which is in contact with the pseudotachylyte. A part of the pseudotachylyte (right end) was removed by mistake while polishing. (c) Pseudotachylyte which fell from the sliding surface during melting. (d) Enlarged picture of (c). The grain size of the fine matrix is still out of the range of measurements at this magnification. **v**; vesicle: **pl**; plagioclase: **k-fel**; k-feldspar: **cpx**; clinopyroxene: **opx**; orthopyroxene: **bt**; biotite and **mt**; magnetite.

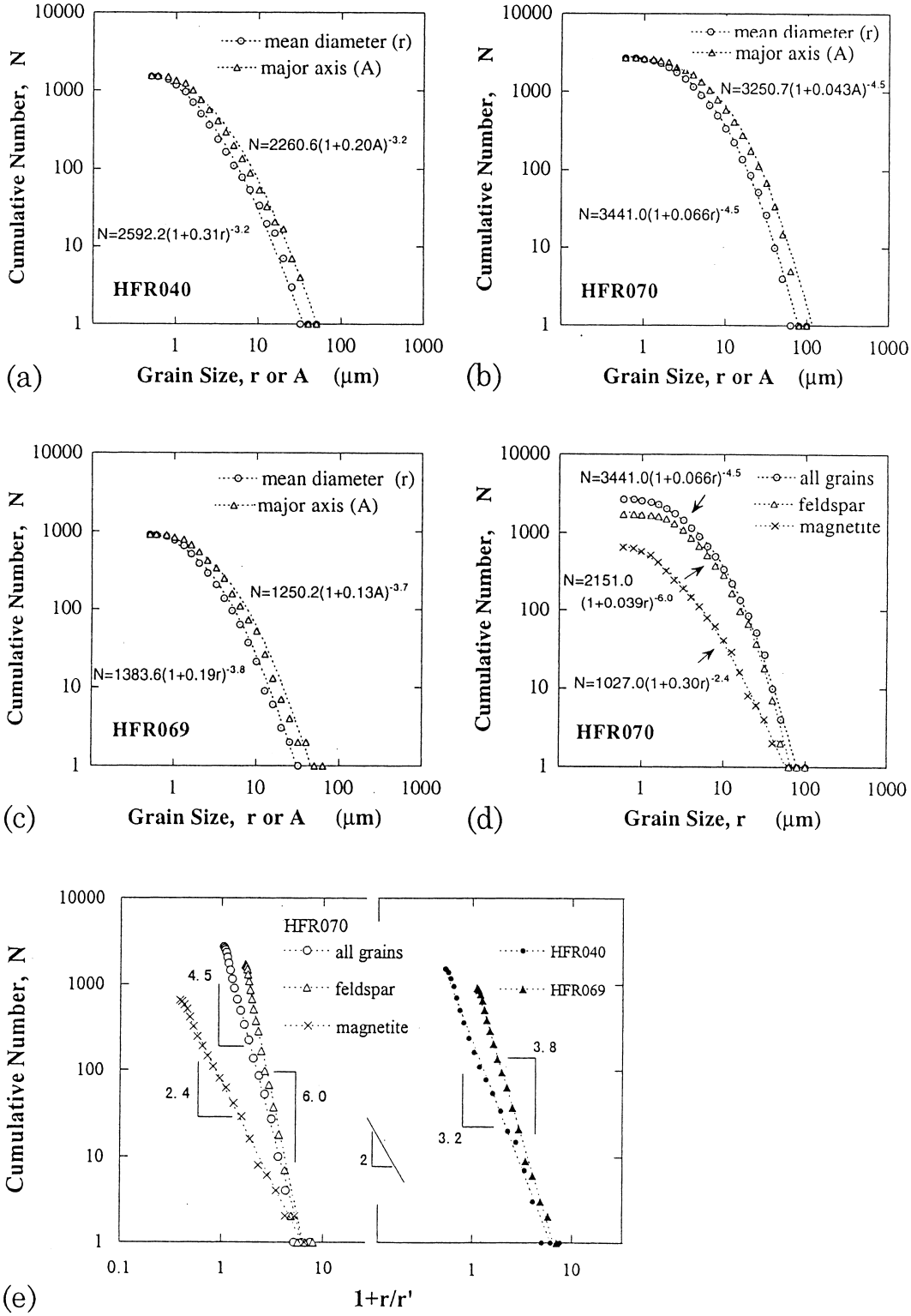


Fig. 2. Cumulative frequency of clast-sizes contained in the experimentally produced pseudotachylyte. $N$ is the cumulative number of clasts whose mean diameter is greater than $r$ (open circle) or whose major axis is greater than $A$ (open triangle). Equations are for best fitting lines to the data, which have the power-law size distribution of Eq. (2) in the text. The minimum size down to which all clasts were measured was 0.5 μm. (a) and (c) Cumulative frequency of clast-sizes contained in two samples of experimentally produced pseudotachylyte on the sliding surface. (b) Size distribution of clasts contained in the experimentally produced pseudotachylyte which fell from the sliding surface during melting. (d) Size distribution of feldspar clasts (open triangle) and that of magnetite clasts (cross) contained in the experimental pseudotachylyte in (b). The frequency of all clasts (open circle) is also shown for comparison. (e) Cumulative frequency of the clasts in the experimental pseudotachylytes plotted against $1+r/r'$. Slope of each plot corresponds to each of the power-law exponents of the regression equations in (a)–(d). A reference line with the slope of 2, i.e. $D=2$, is shown in the figure for comparison.

ately adjacent to the fault zone varies depending upon the mineral species. Pyroxene and magnetite usually show angular surfaces whereas plagioclase, other feldspars and biotite are often characterized by rounded surfaces. The color of the biotite nearest to the fault zone is changed to reddish brown. Some biotite is kinked on the sliding surface or smeared along the sliding surface.

The thin black layer consists of clasts of various sizes and shapes scattered in an ultrafine matrix, and of vesicles (Fig. 1b–d). The clasts are composed of pyroxene, plagioclase, feldspar and magnetite. Optical and SEM-EDS observations reveal that the clasts of biotite are rare in the matrix. The clasts of pyroxene and magnetite are often angular to sub-angular, whereas the clasts of plagioclase and other feldspars are usually rounded in shape.

## 4. The size distribution of clasts

Size distribution analyses were performed on clasts contained in the thin black layer remaining on the simulated fault surfaces (HFR040, HFR069) and those contained in the melt dropped from the sliding surfaces (HFR070). Measurements of clast sizes were made using back scattered electron (BSE) images and the counting method described by Shimamoto and Nagahama (1992). BSE images were found to be an effective tool in this type of analysis, because they permit measurement of the clasts down to 0.1 μm size, and the mineral species of each grain can be easily identified because differences in the color, and gray level, of clasts represent compositional differences (Fig. 1b–d). A lower limit of 0.5 μm was set for the size of the clasts to be measured in order to avoid an oversight of the counting. To avoid biased measurements, the lengths of the major and minor axes of the clasts, $A$ and $B$, respectively, were measured.

The results are plotted as cumulative frequency diagrams for the major axis, $A$, and for the mean diameter, $r$, defined as the geometric mean of $A$ and $B$, using logarithmic scales on both axes of the graph (Fig. 2a–c). Here, $N$ is the cumulative number of clasts whose sizes are greater than $r$ or $A$.

Previous work on the size distributions of clasts in natural pseudotachylytes have found empirically, that the size distribution of the clasts obey either a power-law of the form:

$$N = N' r^{-D} \tag{1}$$

(Okamoto and Kitamura, 1990; Shimamoto and Nagahama, 1992); or the form:

$$N = N'(1 + r/r')^{-D} \tag{2}$$

(Nagahama et al., 1992), where $N'$ and $r'$ are constants. $D$ is a power-law exponent. For the pseudotachylytes experimentally produced in this study, the clasts obey the power-law size distribution of the form identical to Eq. (2) (Fig. 2a–c).

In Fig. 2(d), size distributions of feldspar clasts, magnetite clasts, and all clasts contained in specimen HFR070, are plotted. All these size distributions obey the power law of Eq. (2). The overall form of each of the curves is identical, i.e. they are linear and steep in the coarse-grained size ranges and the slope reduces towards finer size range. The slope of the curve in the coarse-grained size range is steepest for feldspar clasts and shallowest for magnetite clasts. The degree of the flattening of the curve in the fine grain size range is largest for the feldspar clasts and smallest for the magnetite clasts, as can be seen from the difference of $1/r'$ for the curves (Table 1).

## 5. Estimation of the proportion of frictional melt using clast-size data

We shall use the same analysis as Shimamoto and Nagahama (1991, 1992) and Nagahama et al. (1992) for the clasts in experimentally produced pseudotachylytes. Because the area occupied by a particle with size, $r$, is $kr^2$, where $k$ is a shape factor, the total area $S$ occupied by all clasts with sizes ranging from $r_1$ to $r_2$ is given by:

$$\begin{aligned} S &= (kN'D/r') \int_{r_1}^{r_2} r^2 (1 + r/r')^{-(D+1)}\, \mathrm{d} \\ r &= (kN'D/r')[(1 + r/r')^{-D} \{(r'r^2/(2 - D) \\ &\quad - 2r'^3/D(1 - D)(2 - D) - 2r'^2 r/(1 - D \\ &\quad \times 2 - D)\}]_{r_1}^{r_2} \quad (D \neq 1,2). \end{aligned} \tag{3}$$

Equation (3) can be used to test whether the area of matrix of experimental pseudotachylytes is consistent with the predicted area of fine-grained clasts from the size distribution. The values $r_1$ and $r_2$ of the fine-grained size range used in the calculation are shown in Table 1, along with the values $N'$ and $r'$. The minimum size of clasts was assumed arbitrarily as 5 nm (50 Å), a few times larger than the unit cell length of common minerals. The total area of fine-grained clasts of which grain size is in the range of 0.5–0.005 μm predicted using Eq. (3) does not exceed 0.5%, whereas the actual area of the ultrafine-grained matrix of the same specimen is measured to be more than 60%, using a point-counting technique on the BSE photographs (Table 1). For example, the total area of fine-grained clasts in HFR069 is calculated as 0.23%, whereas the actual area of the ultrafine-grained matrix is measured as 67%, a difference of more than two orders of mag-

nitude. A major portion of the matrix cannot therefore be regarded as being of only crush origin.

The size distribution analysis suggests that the 60–70% area of the ultrafine-grained matrix represents the ratio of the produced total melt to the whole products.

## 6. Evaluation of the proportion of frictional melt using X-ray diffraction analysis

Lin (1992, 1994) and Lin and Shimamoto (1994, 1998) proposed a method to evaluate the proportion of glass to the whole products of experimentally and naturally produced pseudotachylytes, by using X-ray diffraction analysis data. Similar analyses have been performed on the experimentally produced pseudotachylytes. The method is only briefly described here, with a more detailed description of the method being given by Lin (1994).

A Philips X-ray diffractometer was used to obtain the diffraction spectra for the experimentally produced pseudotachylytes. A non-refraction specimen holder made of artificial silicon crystal was used to avoid the effects of background glass peaks that can arise when using a conventional glass plate holder. The experimental conditions were: $CuK_{\alpha}$ radiation, X-ray generator 40 kV, 30 mA, and sampling width of 0.02° per one step·s. The X-ray diffraction spectra of the three experimentally produced pseudotachylytes are shown in Fig. 3(a). All of these X-ray diffraction spectra show a broad band background peak ranging from $2\theta = 12°$ to 42°, indicating the existence of glass or amorphous materials. This broad band is also characteristic of natural pseudotachylytes (Lin, 1994) and of experimentally generated pseudotachylytes (Lin and Shimamoto, 1994).

In order to obtain a pure glass sample as a calibration substance for the quantitative analysis of the pseudotachylytes, a monzodiorite sample was completely fused at 1400°C for 3 h and quenched by air. Five standard samples were then prepared, which are made up of 0, 25, 50, 75 and 100% weight of the pure glass by mixing powders of the glass and the host monzodiorite. In Fig. 3(b), X-ray diffraction spectra of the five standard samples are shown. The X-ray diffraction spectra show a broad background peak from $2\theta = 12°$ to 42°, indicating the existence of glass material, similar to that of Fig. 3(a). The integrated intensity ($I_g$) of the broad glass background band, i.e. the shaded area of Fig. 3(b), decreases with decreasing ratio of the

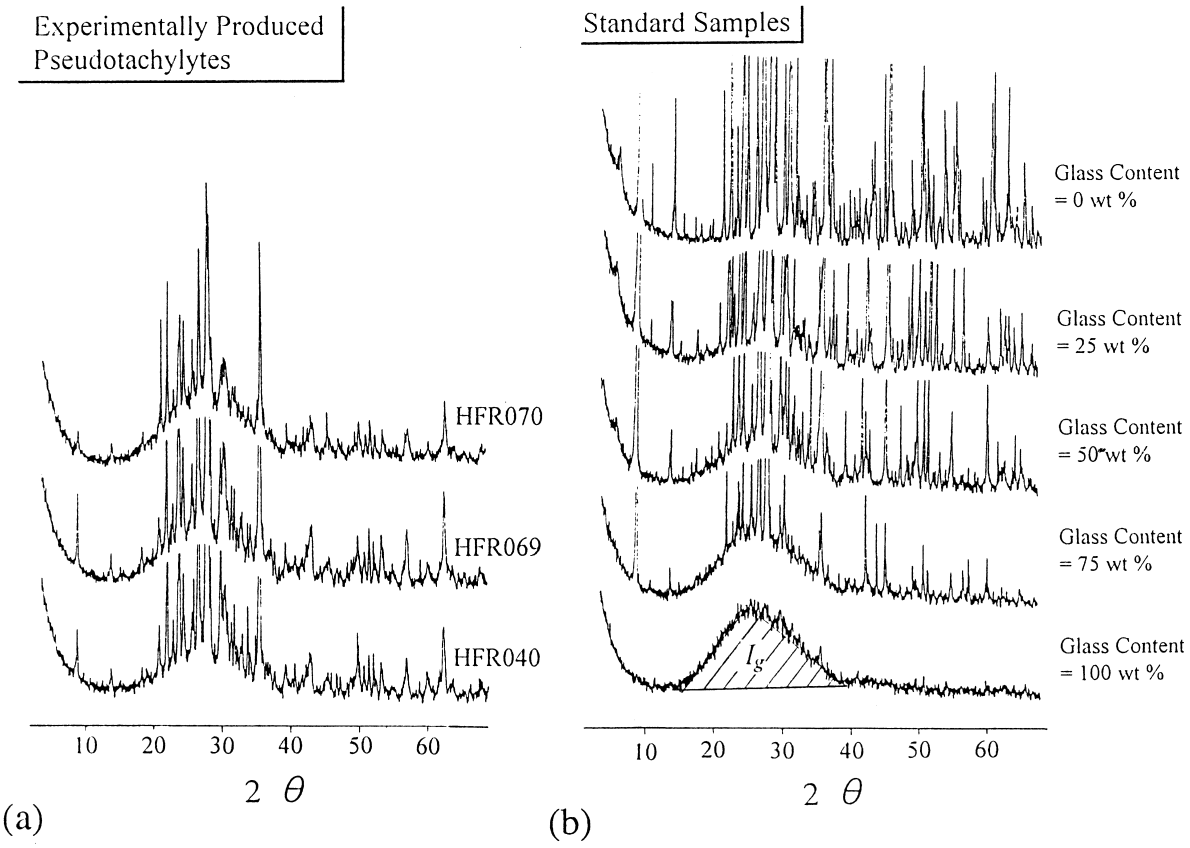


Fig. 3. (a) X-ray spectra of experimentally produced pseudotachylytes from monzodiorite. (b) X-ray spectra of calibration substances.

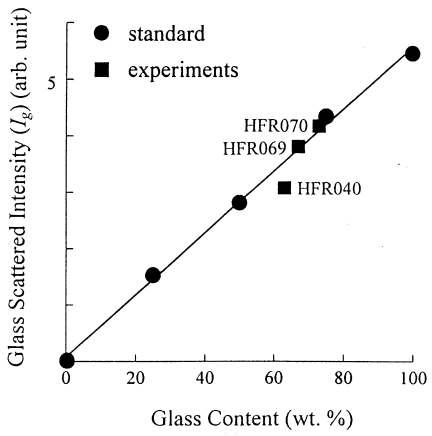


Fig. 4. Plot showing the relationship between the integrated intensity of the glass background peak band on X-ray spectra of the experimental pseudotachylytes (Fig. 3a) and glass contents of the pseudotachylytes predicted from the size distribution analysis data (Table 1). Solid circles represent standard samples which are made of 0–100 wt% of pure glass.

mixed glass contents. In Fig. 4, the integrated intensity of the broad background peak is plotted against the ratio of the mixed glass contents. It shows that there is a linear relationship between the integrated background intensity and the mixed ratio of the glass plots.

If the estimation of the proportion of melt product from the size distribution analysis is correct, then the integrated glass background intensities of the experimentally produced pseudotachylytes (Fig. 3a) and the estimated ratio of the glass matrices using the size distribution analysis (Table 1) should plot near the calibrated line in Fig. 4. In the figure, the integrated intensities and the estimated ratio of the glass of the three specimens are plotted with the calibration data. It is clear that the predicted ratio of the melt matrix to the total products based on the clast-size distribution analysis data is consistent with the calibrated data. It can therefore be concluded that the ultrafine-grained matrix in the experimentally produced pseudotachylytes is almost totally composed of frictional melt.

## 7. Discussion

A critical point regarding the estimation of the proportion of melt product from the size distribution analysis is the size-distribution of ultrafine-grained clasts. As shown in Fig. 2, deviation of the size–frequency curve from a somewhat linear relationship in the coarsest range becomes obvious well within a measurable size range, in which all clasts have been counted. Therefore, at least for the data plotted in Fig. 2, empirical power-law of the form given in Eq. (2) holds. With respect to the size distribution of ultrafine-grained clasts, a detailed discussion has already been made by Shimamoto and Nagahama (1992) on natural pseudotachylytes for various values of the unknown slope of size distribution curves (cf. Shimamoto and Nagahama, 1992, fig. 6). As discussed in their paper, to bring the predicted area of ultrafine-grained clasts into agreement with the measured actual area, the flattened size–frequency curve must change its slope within the ultrafine range of 0.5–0.005 μm to a steep one. This would only be possible if crushing and fragmentation of clasts operated in coarse-grained ranges and severely in the ultrafine range, and thus jumped the size range where the size–frequency curve is flattened. On the contrary, as long as we extrapolate the size distribution of Eq. (2) into ultrafine-grained clasts, any change of $D$ or $r'$ cannot bring predicted and measured areas into agreement because the flattened character of the size–frequency curve in the finer size range never disappears with the change of $D$ or $r'$.

Previous works on the size distribution of clasts in natural fault gouge have found empirically, that the size distribution of clasts produced during comminution processes obeys the power-law of the form identical to Eq. (1), with power-law exponent of $D < 2$ in two dimensions (Sammis et al., 1987; Sammis and Biegel, 1989). The comminution model proposed by Sammis et al. (1987) supports the findings. This model is also supported empirically by experiments on simulated fault gouge (Biegel et al., 1989; Marone and Scholz, 1989). Clasts in the experimental pseudotachylyte, however, obey the power-law of the form in Eq. (2) (Fig. 2e). Its size–frequency curve is linear and steep in the coarse-grained range, but the slope reduces towards the fine-grained range, and eventually becomes almost horizontal (Fig. 2a–d). This suggests that finer-grained clasts were preferentially incorporated into the melt. In specimen HFR070, the rate of flattening of the size–frequency curves in the fine-grained range is the smallest for magnetite clasts. This indicates that magnetite is more resistant than feldspar in grain size reduction processes during melting. The rounded shape of clasts, which is typical of the corrosion texture, is most common for feldspar clasts, while magnetite is characterized by angular grains (Fig. 1). At atmospheric pressure, the melting temperature of magnetite is 1590°C, and of feldspar (andesine, $Ab_{60}An_{40}$) is 1200°C. This suggests that the melting temperature has a major influence on the grain size reduction process of minerals, and therefore on the difference in the rate of flattening between clast size distributions (Fig. 2d).

In the coarse-grained range, the slope of the size–frequency curves of the experimental pseudotachylytes is more than 2 as revealed from the power-law exponent, $D$, of the curves (Fig. 2e). It can be argued that if the refinement process of the clasts in the coarse-grained range is mostly the comminution process, at

least the slope of the curve in the coarse-grained range would become smaller, to a value comparable to that of natural fault gouge. Restricted thickness of the simulated fault zone during frictional melting is inferred to be one of the factors controlling the refinement process of the clasts in the coarse-grained range, and $D$. As shown in Fig. 2, maximum grain size of the clasts in the frictional melt is less than 100 μm, comparable to the thickness of the experimental pseudotachylyte, ca. ~100 μm (Fig. 1). The initial sample, however, contains larger grains; as large as 1 mm or more. If the thickness of the fault zone was much larger than the maximum grain size of the sample, the slope of the coarse-grained size–frequency curve might have become smaller to a value comparable to that of comminution law. Thickness of the fault zone, i.e. thickness of pseudotachylyte melt might strongly depend on the viscosity and thus on the temperature of the melt layer. Thus there may exist a relationship between the slope of the size–frequency curve in the coarse-grained size range and the temperature of the sliding surfaces. More comprehensive work is needed, however, to discuss this problem.

## 8. Conclusions

The results of this study are:

1. The high-speed frictional melting experiments successfully reproduced the geometrical characteristics of the texture of natural pseudotachylytes. The experimentally produced pseudotachylytes consist of clasts of various sizes and shapes in an ultrafine-grained matrix, similar to the textures in the natural pseudotachylytes.
2. The size distribution of clasts in the experimental pseudotachylytes obey the power-law size distribution of the form: $N = N'(1 + r/r')^{-D}$, as has been recognized for natural pseudotachylytes.
3. Analysis of the clast-size distribution data suggests that the total area of ultrafine-grained clasts does not exceed 0.5%, whereas the actual area of the ultrafine-grained matrix is measured to be more than 60% of the total area. The major part of the matrix of the experimentally generated pseudotachylytes cannot therefore be of crush origin. This is consistent with natural pseudotachylyte.
4. The size distribution analysis data suggest that the actual 60–70% area of ultrafine-grained matrix consists mostly of melt (glass). This estimate is consistent with the ratio of glass determined from X-ray diffraction analysis.

## Acknowledgements

Constructive comments about the manuscript from two journal referees D.L. Olgaard and D. Peacock are greatly appreciated. I thank T. Shimamoto, H. Nagahama and A. Lin for their helpful discussions on an earlier stage of this work. K. Nogami is gratefully acknowledged for his help in using XRD. I acknowledge financial support by JSPS Research Fellowships.

## References

Biegel, R.L., Sammis, C.G., Dieterich, J.H., 1989. The frictional properties of a simulated gouge having a fractal particle distribution. Journal of Structural Geology 11, 827–846.

Lin, A., 1992. Experimentally-generated pseudotachylytes. 29th International Geological Congress, vol. 1/3, p. 167.

Lin, A., 1994. Glassy pseudotachylyte veins from the Fuyun fault zone, northwest China. Journal of Structural Geology 16, 71–83.

Lin, A., Shimamoto, T., 1994. Chemical composition of experimentally generated pseudotachylytes. Journal of the Tectonic Research Group of Japan 39, 85–101 (in Japanese with English abstract).

Lin, A., Shimamoto, T., 1998. Selective melting processes as inferred from experimentally generated pseudotachylytes. Journal of Asian Earth Sciences 16, 1–13.

Marone, C., Scholz, C.H., 1989. Particle-size distribution and microstructures within simulated fault gouge. Journal of Structural Geology 11, 799–814.

Nagahama, H., Shimamoto, T., Lin, A., Sato, H., Tsutsumi, A., Ohtomo, Y., Shigematsu, N., Watanabe, T., 1992. Further analysis of clast-size distribution in pseudotachylytes: implication for their origin (Abstract). 29th International Geological Congress, vol. 1/3, p. 169.

Ohtomo, Y., Shimamoto, T., 1994. Significance of thermal fracturing in the generation of fault gouge during rapid fault motion. Journal of the Tectonic Research Group of Japan 39, 135–144 (in Japanese with English abstract).

Okamoto, Y., Kitamura, M., 1990. A mineralogical study of pseudotachylytes from Scotland (Abstract). Annual Meeting of Mineralogical Society of Japan, vol. 47 (in Japanese).

Sammis, C.G., Biegel, R., 1989. Fractals, fault-gouge, and friction. Pure and Applied Geophysics 131, 255–271.

Sammis, C.G., King, G., Biegel, R., 1987. The kinematics of gouge deformation. Pure and Applied Geophysics 125, 777–812.

Shimamoto, T., Nagahama, H., 1991. The origin of pseudotachylytes and the state-of-stress problem. Earth Monthly 13, 416–427 (in Japanese).

Shimamoto, T., Nagahama, H., 1992. An argument against the crush origin of pseudotachylytes based on the analysis of clast-size distribution. Journal of Structural Geology 14, 999–1006.

Shimamoto, T., Tsutsumi, A., 1994. A new rotary-shear high-speed frictional testing machine. Journal of the Tectonic Research Group of Japan 39, 65–78 (in Japanese with English abstract).

Sibson, R.H., 1975. Generation of pseudotachylyte by ancient seismic faulting. Geophysical Journal of the Royal Astronomical Society 43, 775–794.

Tsutsumi, A., Shimamoto, T., 1977. High-velocity frictional properties of gabbro. Geophysical Research Letters 24, 699–702.

Wenk, H.-R., 1978. Are pseudotachylytes products of fracture or fusion? Geology 6, 507–511.